Lattice kinetic scheme for the incompressible viscous thermal flows on arbitrary meshes

Y. Peng, C. Shu, and Y. T. Chew
Department of Mechanical Engineering, National University of Singapore, 10 Kent Ridge Crescent, Singapore 119260, Singapore

T. Inamuro
Department of Chemical Engineering, Kyoto University, Kyoto 606-8501, Japan
(Received 11 June 2003; revised manuscript received 22 August 2003; published 30 January 2004)

A lattice kinetic scheme was developed for the incompressible viscous thermal flows on arbitrary meshes. The work was based on the lattice kinetic scheme proposed by Inamuro and the technique of Taylor series expansion- and least-square–based lattice Boltzmann method (TLLBM). Compared with the lattice Boltzmann method, the lattice kinetic scheme can save the computer memory since there is no need to store the density distributions. The implementation of the boundary condition is direct and just the same as the convectional Navier-Stokes solvers. By using the idea of TLLBM, the lattice kinetic scheme can be applied on arbitrary meshes, which makes this scheme suitable for practical applications. In order to validate this lattice kinetic scheme used on arbitrary meshes, numerical simulations of the natural convection in a square cavity and the natural convection in a concentric annulus between an outer square cylinder and an inner circular cylinder are carried out, and the results are compared very well with available data in the literature.

DOI: 10.1103/PhysRevE.69.016703 PACS number(s): 47.11.+j, 45.50.−j

I. INTRODUCTION

In recent years, the lattice Boltzmann method (LBM) has been developed into an alternative promising tool for fluid mechanics. It has been widely used in many kinds of complex flows such as turbulent flow, multiphase flow, and microflow [1]. However, there are still some items in need of further study. One is the collision model. The Bhatnagar-Gross-Krook (BGK) model with a single relaxation time is usually used for the collision term. The shortcomings of the BGK model are pointed out in the works of d'Humieres [2] and Lallemand and Luo [3]. The other is the boundary condition. The bounce-back scheme in the LBM was originally taken from the LGA method. Although this heuristic scheme is very simple to implement, it is found to be the first order in the numerical accuracy at the boundaries [4,5]. In order to improve the numerical accuracy, other boundary treatments have been proposed. It appears, however, that the extension of these treatments to the complex boundary surface is difficult. Chen *et al.* [6] proposed a boundary condition using a second-order extrapolation scheme of the distributions in the flow to obtain the unknown particle distribution functions on the boundaries. When the flow problems with complex geometries, especially in the three dimensions, are encountered, the determination of the unknown particle directions is troublesome. All the implementations are not so direct since on the boundaries the macroscopic variables, not the density distributions, are given. Related to these two difficulties, a lattice kinetic scheme for the incompressible viscous flows was developed by Inamuro [7]. This scheme is based on the idea that if the dimensionless relaxation time in the LBM with the BGK model is set to unity, the macroscopic variables such as velocity components and density instead of the density distribution functions become the dependent variables in the computation. As compared to the standard LBM, this scheme can save computer memory because there is no need to store the density distribution functions. The implementation of the boundary condition is very easy since on the boundaries only the macroscopic variables rather than the density distributions are needed as for the conventional Navier-Stokes (NS) solvers. This feature is very useful when the flow problems with complex geometry are concerned.

However, since this scheme is in the early stage of the development, its use is currently limited to the two-dimensional uniform grids. When the flow problems with curved boundaries are encountered, the boundaries cannot be well defined when the uniform grids are used. Even when the flows are confined in the regular geometries, nonuniform grid is preferred at high Reynolds number or Rayleigh number. In order to meet these requirements and exploit the good feature of the lattice kinetic scheme in the implementation of the boundary conditions, its extension to the applications on arbitrary meshes is necessary for its development into a competitive method. In this paper, we follow the idea of the Taylor series expansion- and least-square–based LBM (TLLBM) [8–10], and propose a lattice kinetic scheme for its application on the arbitrary mesh. The final form is an algebraic formulation, in which the coefficients only depend on the coordinates of the mesh points and lattice velocity, and can be computed once in advance.

In order to validate our lattice kinetic scheme, the numerical simulations of the natural convection in a square cavity and the natural convection in a concentric annulus between a square outer cylinder and a circular inner cylinder are carried out and compared with available data in the literature.

II. METHODOLOGY

Our lattice kinetic scheme is based on the original lattice kinetic scheme and the idea of TLLBM. Before introducing our lattice kinetic scheme, we will give a brief description about the original lattice kinetic scheme.

A. Original lattice kinetic scheme

The evolution equation for the density distribution $f_\alpha(\mathbf{x},t)$ in the two dimensions with the particle velocity $\mathbf{e}_\alpha$ can be written as

$$f_\alpha(\mathbf{x},t+\delta t)=f_\alpha(\mathbf{x}-\mathbf{e}_\alpha\delta t,t) - \frac{f_\alpha(\mathbf{x}-\mathbf{e}_\alpha\delta t,t)-f_\alpha^{eq}(\mathbf{x}-\mathbf{e}_\alpha\delta t,t)}{\tau}, \quad \alpha=0,1,\ldots,N, \tag{1}$$

where τ is the single relaxation time, f_α^{eq} is the corresponding equilibrium density distribution function, δt is the time step, and N is the number of discrete particle velocities. On the uniform grid, δt is chosen so that the particles travel one-lattice spacing during this time. When the particle velocity model D2Q9, which is defined as

$$\mathbf{e}_\alpha=\begin{cases}\mathbf{0}, & \alpha=0\\ (\cos[(\alpha-1)\pi/2],\sin[(\alpha-1)\pi/2]), & \alpha=1,2,3,4\\ \sqrt{2}(\cos[(\alpha-5)\pi/2+\pi/4],\sin[(\alpha-5)\pi/2+\pi/4]), & \alpha=5,6,7,8\end{cases} \tag{2}$$

is used, a suitable equilibrium distribution function for this model is given by

$$f_\alpha^{eq}=w_\alpha\rho\left[1+3\mathbf{e}_\alpha\cdot\mathbf{V}+\frac{9(\mathbf{e}_\alpha\cdot\mathbf{V})^2}{2}-\frac{3\mathbf{V}^2}{2}\right], \tag{3}$$

where $w_0=4/9$, $w_\alpha=1/9$ for $\alpha=1,2,3,4$, and $w_\alpha=1/36$ for $\alpha=5,6,7,8$. The macroscopic density ρ and fluid velocity $\mathbf{V}$ are calculated in terms of the density distributions as

$$\rho=\sum_{\alpha=0}^{8} f_\alpha, \quad \mathbf{V}=\frac{1}{\rho}\sum_{\alpha=0}^{8} f_\alpha\mathbf{e}_\alpha. \tag{4}$$

The pressure p is related to the density by

$$p=\frac{\rho}{3} \tag{5}$$

and the kinematic viscosity υ is given by

$$\upsilon=\frac{1}{3}\left(\tau-\frac{1}{2}\right)\delta t. \tag{6}$$

When the dimensionless relaxation time τ in Eq. (1) is set to unity, we can obtain

$$f_\alpha(\mathbf{x},t+\delta t)=f_\alpha^{eq}(\mathbf{x}-\mathbf{e}_\alpha\delta t,t). \tag{7}$$

Then using Eq. (4), we can get

$$\rho(\mathbf{x},t+\delta t)=\sum_{\alpha=0}^{8} f_\alpha^{eq}(\mathbf{x}-\mathbf{e}_\alpha\delta t,t),\rho(x,t+\delta t)\mathbf{V}(\mathbf{x},t+\delta t) = \sum_{\alpha=0}^{8} f_\alpha^{eq}(\mathbf{x}-\mathbf{e}_\alpha\delta t,t)\mathbf{e}_\alpha. \tag{8}$$

By using Eqs. (3) and (8), one can calculate the density and fluid velocity without the density distributions. The pressure is obtained with Eq. (5) and the kinematic viscosity is given by

$$\upsilon=\frac{1}{6}\delta t. \tag{9}$$

This may yield a relatively large viscosity.

In order to remove this shortcoming, one can flexibly choose the equilibrium distribution function f_α^{eq} provided that the macroscopic equations recover the NS equations [11]. In this work, the following equilibrium density distribution function given by Inamuro [7] is used:

$$f_\alpha^{eq}=w_\alpha\rho\left[1+3\mathbf{e}_\alpha\cdot\mathbf{V}+\frac{9(\mathbf{e}_\alpha\cdot\mathbf{V})^2}{2}-\frac{3\mathbf{V}^2}{2} + A\,\delta t\left(\frac{\partial u_\delta}{\partial x_\gamma}+\frac{\partial u_\gamma}{\partial x_\delta}\right)e_{\alpha\delta}e_{\alpha\gamma}\right]. \tag{10}$$

The inclusion of the last term in the equilibrium density distribution function is to provide part of the viscous stress tensor in the process of Chapman-Enskog expansion, which can be seen in the following two equations:

$$\Pi_{\alpha\beta}^{(0)}=\sum \mathbf{e}_\alpha\mathbf{e}_\beta f^{eq}=p\,\delta_{\alpha\beta}+\rho u_\alpha u_\beta+\frac{2}{9}\rho A\,\delta t\left(\frac{\partial u_\alpha}{\partial x_\beta}+\frac{\partial u_\beta}{\partial x_\alpha}\right), \tag{11}$$

$$\varepsilon\Pi_{\alpha\beta}^{(1)}=\varepsilon\sum \mathbf{e}_\alpha\mathbf{e}_\beta f^{(1)}=-\rho\left(\tau-\frac{1}{2}\right)c_s^2\,\delta t\left(\frac{\partial u_\alpha}{\partial x_\beta}+\frac{\partial u_\beta}{\partial x_\alpha}\right) \overset{\tau=1}{=} -\rho\frac{1}{6}\delta t\left(\frac{\partial u_\alpha}{\partial x_\beta}+\frac{\partial u_\beta}{\partial x_\alpha}\right). \tag{12}$$

The recovered momentum flux tensor in the Navier-Stokes equations is

$$\Pi_{\alpha\beta}=\Pi_{\alpha\beta}^{(0)}+\varepsilon\Pi_{\alpha\beta}^{(1)}=p\,\delta_{\alpha\beta}+\rho u_\alpha u_\beta + \rho\left(\frac{2}{9}A-\frac{1}{6}\right)\delta t\left(\frac{\partial u_\alpha}{\partial x_\beta}+\frac{\partial u_\beta}{\partial x_\alpha}\right). \tag{13}$$

So, the kinematic viscosity is given by

$$\upsilon=\left(\frac{1}{6}-\frac{2}{9}A\right)\delta t \tag{14}$$

which can avoid the large viscosity by adjusting the parameter of A. The equation system (8) and (10) is called the lattice kinetic scheme.

In the same way, the lattice kinetic scheme for the fluid temperature T can be constructed as

$$T(\mathbf{x},t+\delta t)=\sum_{\alpha=0}^{8} g_\alpha^{eq}(\mathbf{x}-\mathbf{e}_\alpha\delta t,t) \tag{15}$$

with

$$g_\alpha^{eq}=w_\alpha T[1+3\mathbf{e}_\alpha\cdot\mathbf{V}]+w_\alpha B\,\delta t(\mathbf{e}_\alpha\cdot\nabla T). \tag{16}$$

The thermal diffusivity χ of the fluid is given by

$$\chi=\left(\frac{1}{6}-\frac{1}{3}B\right)\delta t. \tag{17}$$

B. New lattice kinetic scheme

In order to extend the use of the original lattice kinetic scheme on the arbitrary mesh, the idea of the TLLBM is introduced in the original lattice kinetic scheme. The TLLBM is based on the standard LBM, the technique of Taylor series expansion and least-squares optimization. The details of TLLBM can be found in [10]. This technique and its derivation procedure can be applied in the lattice kinetic scheme. We will show this in the following.

Suppose that the calculation point is at the grid point $P(x,y,t)$. As seen from Eq. (8), for the original lattice kinetic scheme, the macroscopic density and velocity can be calculated as the function of $f_\alpha^{eq}(x-e_{\alpha x}\delta t,y-e_{\alpha y}\delta t,t)$. For a uniform lattice, $\delta x=e_{\alpha x}\delta t$, $\delta y=e_{\alpha y}\delta t$. So, $(x-e_{\alpha x}\delta t,y-e_{\alpha y}\delta t)$ is at the grid point and the values of $f_\alpha^{eq}(\mathbf{x}-\mathbf{e}_\alpha\delta t,t)$ can be easily determined from Eq. (10). In other words, Eq. (8) can be used to update the density and velocity exactly at the grid points. However, for a nonuniform grid, $(x-e_{\alpha x}\delta t,y-e_{\alpha y}\delta t)$ is usually not at the grid point $(x-\delta x,y-\delta y)$. So the values of $f_\alpha^{eq}(\mathbf{x}-\mathbf{e}_\alpha\delta t,t)$ cannot be obtained from Eq. (10) directly since only the macroscopic properties, such as the density and flow velocity, at every mesh point are known. As a result, the density and velocity at the new time level cannot be obtained using Eq. (8). In order to get the values of $f_\alpha^{eq}(\mathbf{x}-\mathbf{e}_\alpha\delta t,t)$, the Taylor series expansion in the spatial direction is applied.

As shown in Fig. 1, for simplicity, the point P represents the calculation point (x_P,y_P,t), points $A-H$ represent the position $(x_P-e_{\alpha x}\delta t,y_P-e_{\alpha y}\delta t,t)$, and points P_1-P_8 represent the position (x_{P_i},y_{P_i},t) with $x_{P_i}=x_P-\delta x_i$, $y_{P_i}=y_P-\delta y_i$. So, Eq. (8) gives

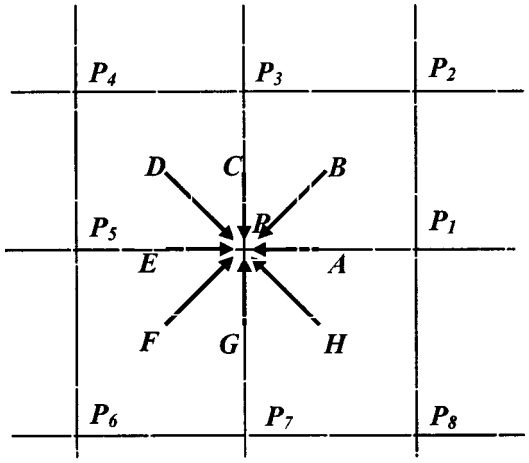

FIG. 1. Configuration at calculation point P.

$$\rho(\mathbf{x},t+\delta t)=\sum_{\alpha=0}^{8} f_\alpha^{eq}(\mathbf{x}_\alpha,t),\rho(\mathbf{x},t+\delta t)\mathbf{V}(\mathbf{x},t+\delta t)$$
$$=\sum_{\alpha=0}^{8} f_\alpha^{eq}(\mathbf{x}_\alpha,t)\mathbf{e}_\alpha, \tag{18}$$

where $\mathbf{x}_0=P$, $\mathbf{x}_1=E$, $\mathbf{x}_2=F$, $\mathbf{x}_3=G$, $\mathbf{x}_4=H$, $\mathbf{x}_5=A$, $\mathbf{x}_6=B$, $\mathbf{x}_7=C$, and $\mathbf{x}_8=D$.

For the general case, $A-H$ may not coincide with the mesh points P_1-P_8. We will take the point F as an example. F may not coincide with the mesh point P_6. Since $f_\alpha^{eq}(P_6,t)$ is known, we can build the connection between $f_\alpha^{eq}(F,t)$ and $f_\alpha^{eq}(P_6,t)$ by using the Taylor series expansion to the second order derivative terms. That is

$$f_\alpha^{eq}(P_6,t)=f_\alpha^{eq}(F,t)+\Delta x_{P_6}\frac{\partial f_\alpha^{eq}(F,t)}{\partial x}+\Delta y_{P_6}\frac{\partial f_\alpha^{eq}(F,t)}{\partial y}$$
$$+\frac{1}{2}(\Delta x_{P_6})^2\frac{\partial^2 f_\alpha^{eq}(F,t)}{\partial x^2}$$
$$+\frac{1}{2}(\Delta y_{P_6})^2\frac{\partial^2 f_\alpha^{eq}(F,t)}{\partial y^2}$$
$$+\Delta x_{P_6}\Delta y_{P_6}\frac{\partial^2 f_\alpha^{eq}(F,t)}{\partial x\partial y}$$
$$+O[(\Delta x_{P_6})^3,(\Delta y_{P_6})^3], \tag{19}$$

where $\Delta x_{P_6}=x_{P_6}-(x_P-e_{\alpha x}\delta t)$, $\Delta y_{P_6}=y_{P_6}-(y_P-e_{\alpha y}\delta t)$. For the two-dimensional case, this expansion involves six unknowns, that is, one equilibrium distribution function at the point F, two first order derivatives, and three second-order derivatives at this point. To solve for these unknowns, six equations are needed to close the system. This can be done by applying the second order Taylor series expansion at six points: P,P_3,P_4,P_5,P_6,P_7. The following equation system can be obtained:

$$f'_k=\{s_k\}^T\{W\}=\sum_{j=1}^{6} s_{k,j}W_j, \quad k=P,P_3,P_4,P_5,P_6,P_7, \tag{20}$$

where

$$f'_k=f^{eq}_\alpha(x_k,y_k,t),$$

$$\{s_k\}^T=\{1,\Delta x_k,\Delta y_k,(\Delta x_k)^2/2,(\Delta y_k)^2/2,\Delta x_k\Delta y_k\}$$

$$\{W\}=\{f^{eq}_\alpha,\partial f^{eq}_\alpha/\partial x,\partial f^{eq}_\alpha/\partial y,\partial^2 f^{eq}_\alpha/\partial x^2,\partial^2 f^{eq}_\alpha/\partial^2 y,$$
$$\partial^2 f^{eq}_\alpha/\partial x\partial y\}^T.$$

Our target is to find the first element $W_1=f^{eq}_\alpha(F,t)$. Equation system (20) can be put into the following matrix form:

$$[S]\{W\}=\{f'\}, \tag{21}$$

where $[S]$ is a matrix formed by the vector $\{s_k\}$. In practical applications, it was found that the matrix $[S]$ might be singular or ill-conditioned using only six points (P, P_3, P_4, P_5, P_6, and P_7). To overcome this difficulty and make the method be more general, more points are added and the least-squares approach [12] was introduced to optimize the overconstrained approximation by Eq. (20). As a result, the equation system for $\{W\}$ becomes

$$\{W\}=([S]^T[S])^{-1}[S]^T\{f'\}=[A]\{f'\}. \tag{22}$$

From Eq. (22) we can have

$$f^{eq}_\alpha(F,t)=W_1=\sum_{k=0}^{M-1} a_{1,k}f'_k, \tag{23}$$

where $a_{1,k}$ are the elements of the first row of the matrix $[A]$, which is determined by the coordinates of the mesh points, the particle velocity, and time step size, and will not be changed in the calculation procedure, and M is the number of the points used and should be greater than 6. In the present study, a structured grid is used, and M is taken as 9. This means that for a reference mesh point P, we need to select its eight neighboring points to compute the coefficients in Eq. (23). The above procedure shows the calculation of $f^{eq}_\alpha(F,t)$ and the same procedure can be applied to calculate the equilibrium distribution function at other points such as A, B, C, and so on. Then the density and velocity can be obtained by

$$\rho(\mathbf{x},t+\delta t)=\sum_{A-H}\sum_{k=0}^{M-1} a_{1,k}f'_k,\rho(\mathbf{x},t+\delta t)\mathbf{V}(\mathbf{x},t+\delta t)$$
$$=\sum_{A-H}\sum_{k=0}^{M-1} a_{1,k}f'_k\mathbf{e}_\alpha. \tag{24}$$

We can calculate the coefficients in Eq. (24) once and store them in advance, so little computational effort is introduced as compared with the original lattice kinetic scheme. On the other hand, Eq. (24) has nothing to do with the mesh structure. It only needs the information of coordinates of the mesh points. Thus, we can say that Eq. (24) can be consistently used to any kind of mesh structure. But we have to indicate that, as compared to the original lattice kinetic scheme, the present method requires much more memory to store the coefficients $a_{1,k}$. This is the price paid for its application to arbitrary mesh.

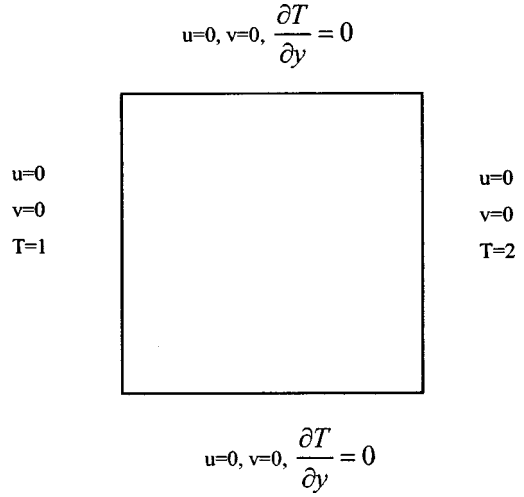

FIG. 2. Configuration of natural convection in a square cavity.

The same procedure can be applied to the calculation of $g^{eq}_\alpha(\mathbf{x}-\mathbf{e}_\alpha\delta t,t)$ so that the temperature can be obtained. If we use the same particle velocity model and neighboring points, the geometry matrix is the same as for $f^{eq}_\alpha(\mathbf{x}-\mathbf{e}_\alpha\delta t,t)$, which can save the computational time and memory space. The temperature can be obtained by

$$T(\mathbf{x},t+\delta t)=\sum_{A-H}\sum_{k=0}^{M-1} a_{1,k}g'_k, \tag{25}$$

where $g'_k=g^{eq}_\alpha(x_k,y_k,t)$. Thus the equation systems (10), (14), (24) for the density, velocity, and (16), (17), (25) for the temperature form our new lattice kinetic scheme.

III. BOUNDARY CONDITIONS

On the boundaries, usually the macroscopic variables and their first order derivatives are specified. These conditions can be implemented for the lattice kinetic scheme in the same way as for the conventional computational fluid

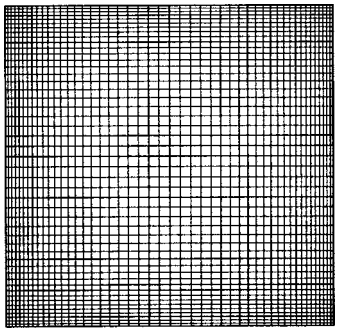

FIG. 3. A typical nonuniform mesh in a square cavity.

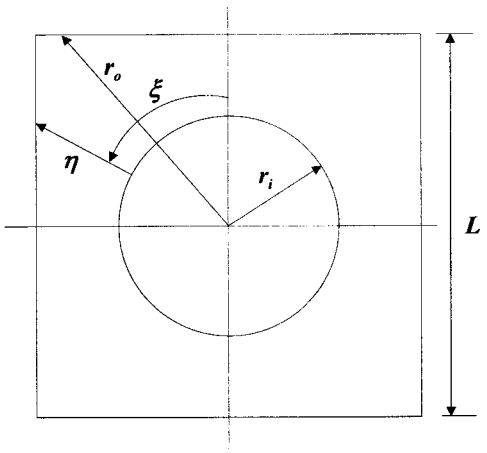

FIG. 4. Sketch of the physical domain.

dynamics (CFD) solvers. This is one of the attracting advantages of the lattice kinetic scheme over the standard LBM.

IV. NUMERICAL SIMULATIONS

In order to examine the accuracy of the lattice kinetic scheme to solve the incompressible thermal flows on the arbitrary meshes, two test problems are calculated. One is the natural convection in a square cavity. The top and bottom walls are insulated and the side walls are maintained at constant but different temperatures. The problem definition and the boundary conditions are displayed in Fig. 2. The nonuniform grid is used and a typical nonuniform grid is shown in Fig. 3. It can be seen clearly from Fig. 3 that the mesh points are stretched near the walls to capture the thin boundary layer. In the middle part of the flow field, the mesh is relatively coarse since the velocity and temperature gradients are not very large in this region. The other is the natural convection in a concentric annulus between an outer square cylinder and an inner circular cylinder. Heat is generated uniformly within the circular inner cylinder with high temperature $T_2=2$, which is placed concentrically within the cold square cylinder with temperature $T_1=1$. A schematic view of the geometry of this problem is shown in Fig. 4. The nonuniform grid, in which mesh points are stretched near the walls, is adopted. The reason to choose this case is to testify the validity of the lattice kinetic scheme to solve the thermal problems with curved boundaries. When the curve boundary is involved and the bounce back boundary condition is to be used, as shown in [10], the determination of the directions where the density distributions are unknown is time consuming and troublesome. When the lattice kinetic scheme is applied, this problem can be avoided.

For the natural convection, the Boussinesq approximation is applied to the buoyancy force term. This means that the properties β and υ are considered as constants, the density ρ is constant, and the buoyancy term is assumed to depend linearly on the temperature,

$$\rho\mathbf{G}=\rho\beta g_0(T-T_m)\mathbf{j}, \tag{26}$$

where β is the thermal expansion coefficient, g_0 is the acceleration due to the gravity, $T_m=(T_1+T_2)/2$ is the average temperature, in which T_1 and T_2 are low and high temperatures, respectively, and $\mathbf{j}$ is the vertical direction opposite to that of the gravity. Correspondingly, the external force term $3w_\alpha g_0\beta(T-T_m)e_{\alpha y}\delta t$ is added to the density equilibrium distribution function (10).

The dimensionless parameters for the natural convection problems are the Prandtl number Pr and the Rayleigh number Ra, defined by

$$\mathrm{Pr}=\upsilon/\chi, \tag{27}$$

$$\mathrm{Ra}=\frac{\beta(T_2-T_1)g_0L^3}{\upsilon\chi}=\frac{\beta\Delta T g_0L^3}{\upsilon\chi}. \tag{28}$$

For the natural convection in a square cavity, L is the height of the square cavity, while for the natural convection in a concentric annulus between an outer square cylinder and an inner circular cylinder, L is the side length of the square cylinder.

In Eq. (28), $\sqrt{\beta g_0\Delta TL}$ is the characteristic velocity. To ensure the code working properly in the near-incompressible regime, the value of $\sqrt{\beta g_0\Delta TL}$ should be carefully chosen. It is chosen to be 0.1 at low Rayleigh number and be 0.15 at high Rayleigh number. This means that the Mach number is 0.1 at low Rayleigh number and 0.15 at high Rayleigh number.

Once the two dimensionless parameters Pr and Ra are given, the kinematic viscosity and thermal diffusivity are determined by solving Eqs. (27) and (28). Then the two

TABLE I. Comparison of numerical results between the lattice kinetic scheme and a Navier-Stokes solver.

Ra	10^3		10^4		10^5		10^6	
Method	Present	[13]	Present	[13]	Present	[13]	Present	[13]
Grid size	101×101		101×101		151×151		201×201	
$u_{\max}$	3.653	3.649	16.224	16.190	34.467	34.736	64.779	64.775
Y	0.815	0.815	0.825	0.825	0.853	0.855	0.857	0.850
$\nu_{\max}$	3.706	3.698	19.779	19.638	69.667	68.640	225.471	220.64
X	0.176	0.180	0.121	0.120	0.066	0.065	0.037	0.035
$\overline{\mathrm{Nu}}$	1.118	1.118	2.250	2.245	4.533	4.523	8.900	8.800
$\lvert\psi_{\mathrm{mid}}\rvert$	1.176	1.175	5.090	5.075	9.118	9.117	16.640	16.270

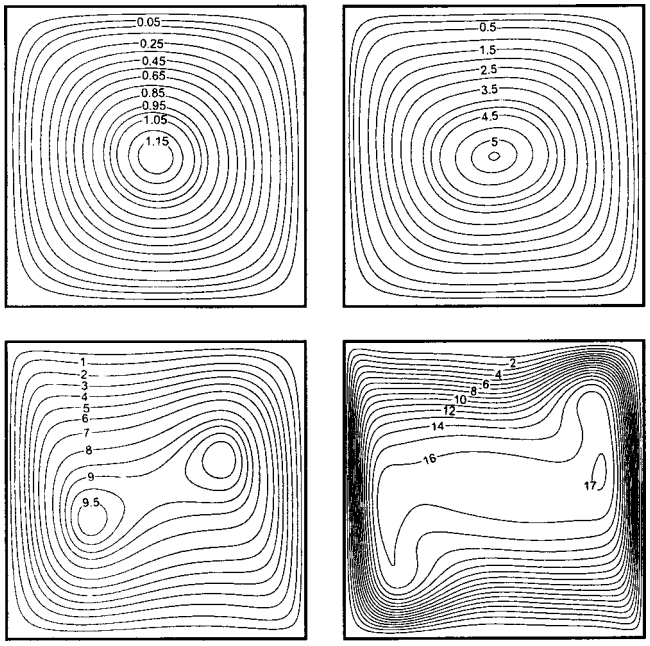

FIG. 5. Streamlines for natural convection in a square cavity at $\mathrm{Ra}=10^3$, 10^4, 10^5, and 10^6.

parameters A and B in Eqs. (10) and (16) can be determined through the relationships expressed by Eqs. (14) and (17).

The convergence criterion for all the cases is set to

$$\max\left|\sqrt{(u_{i,j}^2+\nu_{i,j}^2)^{n+1}}-\sqrt{(u_{i,j}^2+\nu_{i,j}^2)^{n}}\right| \leqslant 10^{-7}, \max\left|T_{i,j}^{n+1}-T_{i,j}^{n}\right|\leqslant 10^{-7}, \tag{29}$$

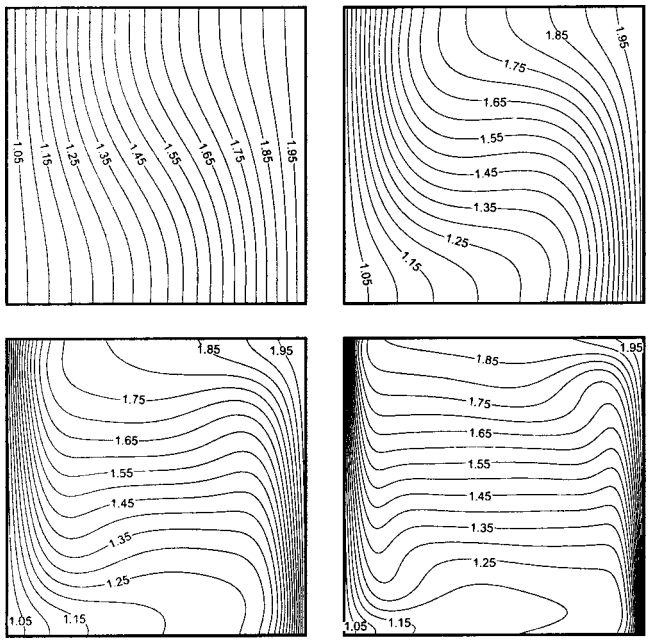

FIG. 6. Isotherms for natural convection in a square cavity at $\mathrm{Ra}=10^3$, 10^4, 10^5, and 10^6.

TABLE II. Comparison of $\psi_{\max}$ $\overline{\mathrm{Nu}}$ for the natural convection in an annulus between an outer square cylinder and a heated inner circular cylinder.

		$\psi_{\max}$		$\overline{\mathrm{Nu}}$	
Ra	Grid	Present	[15]	Present	[15]
10^4	201×61	0.96	0.97	3.23	3.24
5×10^4	241×121	4.83	4.82	4.03	4.02
10^5	241×121	8.19	8.10	4.89	4.86

where n and $n+1$ represent the old and new time levels, respectively.

A. Natural convection in a square cavity

Numerical simulations for the natural convection in a square cavity at a wide range of Rayleigh numbers from 10^3 to 10^6 on the nonuniform grids were carried out.

1. Definition of the Nusselt number

Nusselt number Nu is one of the most important dimensionless parameters in describing the convective heat transport. Its average in the whole flow domain and along the vertical line of $x=x_0$ can be defined by

$$\overline{\mathrm{Nu}}=\frac{L}{\chi\Delta T}\frac{1}{L^2}\int_0^L\int_0^L q_x(x,y)\,dx\,dy, \tag{30}$$

$$\mathrm{Nu}=\frac{L}{\chi\Delta T}\frac{1}{L}\int_0^L q_x(x_0,y)\,dy, \tag{31}$$

where $q_x(x,y)=uT(x,y)-\chi(\partial/\partial x)T(x,y)$ is the local heat flux in the horizontal direction.

2. Validation of the numerical results

Table I shows the numerical results of the maximum horizontal velocity $u_{\max}$ on the vertical midplane of the cavity and its location Y, the maximum vertical velocity $\nu_{\max}$ on the horizontal midplane of the cavity and its location X, the average Nusselt number throughout the cavity $\overline{\mathrm{Nu}}$, and the value of the stream function at the center point of the cavity for a wide range of Rayleigh numbers. The numerical results of the Navier-Stokes equations given by Shu and Xue [13] using the differential quadrature (DQ) method are also included for comparison. From this table, we can see that our numerical results using the lattice kinetic scheme agree very well with the benchmark results. This shows the validity of the use of the lattice kinetic scheme on the nonuniform grids.

Figures 5 and 6 show the corresponding streamlines and isotherms at $\mathrm{Ra}=10^3$, 10^4, 10^5, and 10^6. For $\mathrm{Ra}=10^3$, the stream function value is in the range of 0–1.176. The maximum stream functions are 5.096, 9.651, and 16.890 for $\mathrm{Ra}=10^4-10^6$, respectively. These plots agree well with those obtained by Shu and Xue [13].

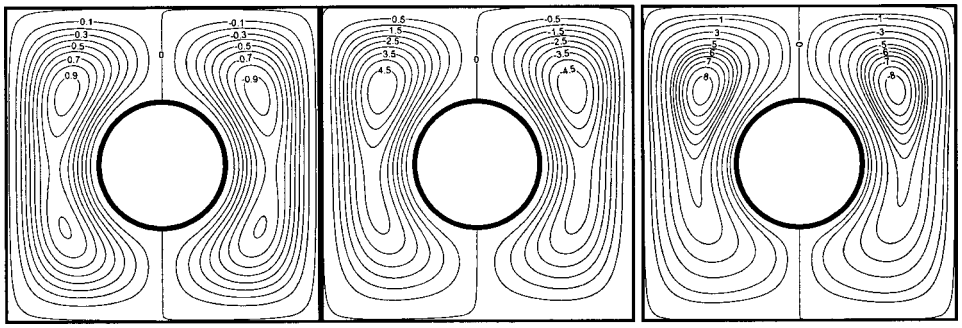

FIG. 7. Streamlines for the natural convection in a concentric annulus between a square outer cylinder and a circular inner cylinder at $\mathrm{Ra}=10^4$, 5×10^4, and 10^5.

B. Natural convection in a concentric annulus between an outer square cylinder and an inner circular cylinder

Numerical simulations of the natural convection in a concentric annulus between an outer square cylinder and an inner circular cylinder were carried out at various Rayleigh numbers. The geometry ratio between the square cylinder and circular cylinder is defined as $rr=L/2r_i$ and is fixed at 2.5 in the present work.

1. Definition of the Nusselt number

The local heat transfer rate on the inner cylinder can be computed by

$$q=h(T_2^*-T_1^*)=-k\frac{\partial T^*}{\partial n}, \tag{32}$$

where T^* is the dimensional temperature, T_2^*, T_1^* are, respectively, the temperatures on the inner and outer walls, h represents the local heat transfer coefficient, and k is the thermal conductivity. From Eq. (32) we can get

$$h=-k\frac{\partial T}{\partial n}. \tag{33}$$

Here T is the nondimensional temperature, which is defined as $T=(T^*-T_1^*)/(T_2^*-T_1^*)$ and $\partial T/\partial n$ is the temperature gradient in the direction normal to the boundary.

Since at the steady state, the Nusselt numbers along the inner and outer walls are the same, there is no need to pay separate attention to the average Nusselt numbers for the outer and inner boundaries. The average Nusselt number for the inner boundary is determined by

$$\overline{\mathrm{Nu}}=\frac{\overline{hS}}{k}=\frac{\overline{\partial T}}{\partial n}S, \tag{34}$$

where S is defined as half of the circumferential length of the inner cylinder surface due to the symmetry, which is the same as in the work of Moukalled and Acharya [14] for the purpose of comparison, and $\overline{h}$ is the average heat flux along the boundary.

2. Validation of the numerical results

The numerical results of the maximum stream function $\psi_{\max}$ and the average Nusselt number $\overline{\mathrm{Nu}}$ for Rayleigh numbers of 10^4 to 10^5 at the geometry ratio of 2.5 are shown in Table II. The benchmark results using the DQ method [15] are also included for comparison. From this table we can see that the numerical results using new lattice kinetic scheme agree very well with the benchmark results. This validates the use of the lattice kinetic scheme on the arbitrary meshes with curved boundaries.

The respective streamlines and isotherms are shown in Figs. 7 and 8. For $\mathrm{Ra}=10^4$, the stream function value is in the range of $(-0.96–0.96)$. The stream functions are in the ranges of $(-4.83–4.83)$ and $(-8.19–8.19)$ for $\mathrm{Ra}=5\times10^4$ and 10^5, respectively. They are in good agreement with the plots shown in [15].

V. CONCLUSIONS

A lattice kinetic scheme for the incompressible viscous thermal flows on the arbitrary meshes is developed following the original lattice kinetic scheme and the idea of TLLBM. The numerical results of the natural convection in a square cavity and the natural convection in a concentric annulus

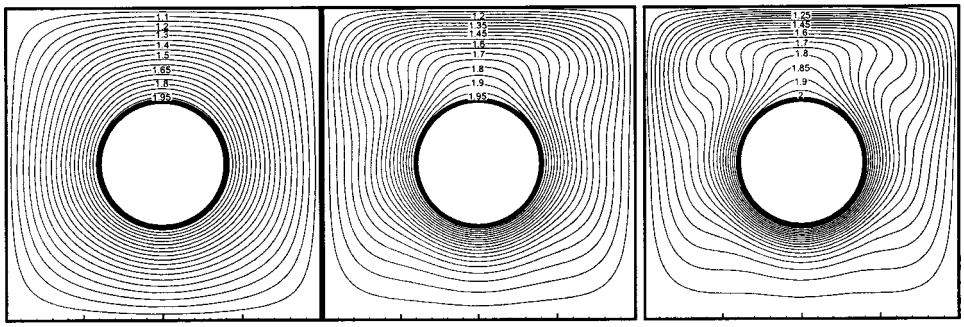

FIG. 8. Isotherms for natural convection in a concentric annulus between a square outer cylinder and a circular inner cylinder at $\mathrm{Ra}=10^4$, 5×10^4, and 10^5.

between an outer square cylinder and an inner circular cylinder validate the use of the lattice kinetic scheme on the arbitrary meshes. This scheme has the following good features. On one hand, it can save the memory space as compared with TLLBM, since there is no need to store the distribution functions. On the other hand, the implementation of the boundary condition becomes easier and more direct, especially in the presence of curve boundaries. These good features and the preliminary calculations show that this scheme is very suitable for practical applications.

[1] S. Chen and G. D. Doolen, Annu. Rev. Fluid Mech. **30**, 329 (1998).
[2] D. d'Humieres, in *Rarefied Gas Dynamics: Theory and Simulations*, edited by B. D. Shizgal and D. P. Weaver, Progress in Astronautics and Aeronautics Vol. 159 (AIAA, Washington, D.C., 1992), pp. 450–458.
[3] P. Lallemand and L.-S. Luo, Phys. Rev. E **61**, 6546 (2002).
[4] R. Cornubert, D. d'Humieres, and D. Levermore, Physica D **47**, 241 (1991).
[5] D. P. Ziegler, J. Stat. Phys. **71**, 1171 (1993).
[6] S. Chen, D. Martinez, and R. Mei, Phys. Fluids **8**, 2527 (1996).
[7] T. Inamuro, Philos. Trans. R. Soc. London, Ser. A **360**, 477 (2002).
[8] C. Shu, Y. T. Chew, and X. D. Niu, Phys. Rev. E **64**, 045701 (2001).
[9] Y. T. Chew, C. Shu, and X. D. Niu, Int. J. Mod. Phys. C **13**, 719 (2002).
[10] Y. Peng, Y. T. Chew, and C. Shu, Phys. Rev. E **67**, 026701 (2003).
[11] S. Succi, *The Lattice Boltzmann Equation for Fluid Dynamics and Beyond* (Oxford University Press, New York, 2001), Chap. 4, pp. 62 and 63.
[12] G. H. Golub and C. F. Van Loan, Matrix Computations, 3rd ed. (Johns Hopkins University Press, Baltimore, 1996).
[13] C. Shu and H. Xue, Int. J. Heat Fluid Flow **19**, 59 (1998).
[14] F. Moukalled and S. Acharya, J. Thermophys. Heat Transfer **10**, 524 (1996).
[15] C. Shu and Y. Zhu, Int. J. Numer. Methods Fluids **38**, 429 (2002).